Pseudogap phase and fractionalization: Predictions for Josephson junction setup

Anurag Banerjee [ORCID],[1] Alvaro Ferraz,[2] and Catherine Pépin[1]

[1]*Institut de Physique Théorique, Université Paris-Saclay, CEA, CNRS, F-91191 Gif-sur-Yvette, France*
[2]*International Institute of Physics - UFRN, Natal, Brazil*

The pseudogap regime of the underdoped cuprates arguably remains one of the most enigmatic phenomena of correlated quantum matter. Recent theoretical ideas suggest that a pair density wave (PDW) or a "fractionalized PDW" could be a key ingredient for the understanding of the pseudogap physics. These ideas are to be contrasted to the scenario where charge density wave order and superconductivity coexist at low temperatures. In this paper, we present a few tests to compare the two scenarios in a Josephson junction setup. For a PDW scenario, we observe a beatlike structure of AC Josephson current. The additional frequencies for the AC Josephson current appear at the half-odd integer multiple of the standard Josephson frequency. We can extract the modulation wave vector of the PDW state by studying the average Josephson current. Furthermore, the usual sharp Shapiro steps break down. In contrast, these signatures are absent for the simple coexistence of orders. Any detection of such signatures in a similar experimental setup will strongly support the PDW scenario for the pseudogap phase.

I. INTRODUCTION

One of the most unusual features of the cuprates is the proliferation of quasidegenerate orders in the underdoped regime near the mysterious pseudogap (PG) phase [1–3]. These include experimentally established orders, such as superconductivity (SC), charge density wave (CDW), and antiferromagnetism. Additionally, it may also harbor putative "hidden" orders such as the pair density wave (PDW) state, for which experimental evidence is still lacking. Conceptually, it is natural to advocate that a very unusual interplay of states is responsible for the formation of the PG [4]. Many routes are proposed to drive forward this set of ideas.

First, there are the proposals of a vestigial order [5–10]. In this framework, the system forms all the potentially degenerate orders. These orders compete within a standard Ginzburg-Landau description, resulting in some precursor order that can account for the development of the pseudogap state. For example, in this scenario, the competition between the SC and CDW state can lead to a precursor state formed by a long-ranged PDW order [11–13].

A more unconventional proposal affirms that such appearance of quasidegenerate states can lead to an emergent symmetry [14–20]. Concretely, considering only the SC and CDW orders for simplicity, the corresponding emergent symmetry is the SU(2) group, rotating between the two states. However, this emergent symmetry is fragile and it is easily destroyed by a slight tuning of appropriate parameters. Nevertheless, the idea of an emergent symmetry is the first illustration of the presence of some entangled states, in this particular case the SC and CDW states, which is undoubtedly present in the cuprates. Indeed some proposals have suggested that around optimal doping, the cuprate superconductors form a maximally entangled state which is associated with a strong-coupling fixed point that can be accessed within the holographic framework [21].

Somewhere in between the ideas of an ultimately entangled fixed point and a vestigial order remains yet another proposal [22–25]. In this approach, at T^* the system is ripe to form all possible particle-particle (PP) and particle-hole (PH) pairs that symmetry allows. This includes PP pairs with zero and finite momentum, and PH pairs with finite momentum, some of which are magnetically inert and others active. Some preformed pairs become unstable and fractionalize into more robust pairs at lower temperatures. A gauge field emerges, and the corresponding constraint generated by the fluctuations leads to the opening of a gap and, thus, to the pseudogap phase itself. The rest of the introduction highlights the critical differences between fractionalized PDW and coexisting order scenarios.

A. Theoretical concepts for "fractionalized" PDW and coexisting orders

We focus on the idea of a PDW preformed pair, fractionalizing into a CDW and SC pairs. The choice has the advantage of simplicity since these two orders are ubiquitously observed [26–31] inside the PG region. The CDW pair is given by $\hat{\chi}_{ij} = g_\chi \hat{d}_{ij} \sum_\sigma c^\dagger_{\mathbf{i},\sigma} c_{\mathbf{j},\sigma} e^{i\mathbf{Q}_0 \cdot (\mathbf{r_i}+\mathbf{r_j})/2}$, where i, j are the nearest-neighbor bonds with $\mathbf{Q}_0$ being the modulation wave vector, and g_χ the interaction responsible for forming CDW pairs. $\hat{d}_{ij}$ is the form factor with a d-wave symmetry. Similarly, the SC pairs are defined as $\hat{\Delta}_{ij} = g_\Delta \hat{d}_{ij} \sum_\sigma \sigma c_{i,\sigma} c_{j,-\sigma}$, where $c^\dagger$ (c) are the standard creation (annihilation) operators for electrons and g_Δ is the interaction forming the Cooper pairs. The origin of such unstable boson at high temperature most certainly comes from the strong-coupling regime of the electrons [32–34] but this is not the main focus of the paper. The PDW is

defined as $\hat{\Delta}_{PDW} = g_{PDW} c_{i\downarrow} c_{i\uparrow} e^{i\mathbf{Q}_0 \cdot (\mathbf{r}_i + \mathbf{r}_j)/2}$. It turns out that it can be written as a combination of elementary operators, i.e., $\hat{\Delta}^*_{PDW} = \frac{g_{PDW}}{2g_\Delta g_\chi} [\hat{\Delta}_{ij}, \hat{\chi}^*_{ij}]$ and $\hat{\Delta}_{PDW} = \frac{g_{PDW}}{2g_\Delta g_\chi} [\hat{\chi}_{ij}, \hat{\Delta}^*_{ij}]$ where $[a, b]$ stands for the commutator of the operators a and b.

The key idea leading to the fractionalization of the PDW is that at the PG temperature T^* a gauge field (or, equivalently, a local phase) emerges,

$$\hat{\Delta}_{ij} \to \hat{\Delta}_r e^{i\theta_{ij}}, \quad \hat{\chi}_{ij} \to \hat{\chi}_r e^{i\theta_{ij}}, \tag{1}$$

and $\hat{\Delta}_{PDW}$ and $\hat{\Delta}^*_{PDW}$ remain invariant under these transformations. Fluctuations of the gauge field in an effective field theory generates a constraint (note that the Δ and χ have the dimension of energy)

$$|\Delta_r|^2 + |\chi_r|^2 = (E^*)^2, \tag{2}$$

where E^* is an energy scale typical of the PG, which is constant in temperature, and with respect to spatial variations, but doping dependent. Note that Δ_r (χ_r) is the local expectation value of $\hat{\Delta}$ ($\hat{\chi}$) at position r. When the coupling to the conduction electrons is considered, the constraint of Eq. (2) opens a gap, primarily in the antinodal (AN) region of the Fermi surface, leading to the presence of Fermi arcs in the nodal region [22–25]. In the temperature regime $T^* > T > T_{co}$, the spatial expectation values of $\langle \Delta_r \rangle = 0$ and $\langle \chi_r \rangle = 0$ as well as the relative phase remain fluctuating.

The typical effective field theory describing the $\hat{\Delta}_{PDW}$ mode has the form of a quantum rotor model [22]

$$S = \frac{1}{2} \int d^2 x \sum_{a,b=1}^{2} |\omega_{ab}|^2,$$
$$\text{with} \quad \omega_{ab} = z_a \partial_\mu z_b - z_b \partial_\mu z_a, \tag{3}$$

with $z_1 = \Delta/E^*$, $z_2 = \chi/E^*$, $z_1^* = \Delta^*/E^*$, $z_2^* = \chi^*/E^*$. Note that E^* is a real quantity associated with the PG energy scale. The gauge fluctuations within the transformation $z_a \to z_a e^{i\theta}$, ($z_a^* \to z_a^* e^{-i\theta}$) are naturally described by the constraint $\sum_a |z_a|^2 = C$ (where C is a constant), equivalent to Eq. (2). The model Eq. (3) is formally equivalent to the CP^1 model,

$$S = \int d^2 x |D_\mu \psi|^2,$$
$$\text{with} \quad D_\mu = \partial_\mu - i\alpha_\mu,$$
$$\text{and} \quad \alpha_\mu = \frac{1}{2} \sum_a z_a^* \partial_\mu z_a - z_a \partial_\mu z_a^*, \tag{4}$$

with $\psi = (z_1, z_2)^T$ [35]. The model in Eq. (4) is, in turn, almost the same as a nonlinear σ model, but with an additional gauge field α taking care of the intrinsic U(1) gauge symmetry.

By contrast in the model of coexisting phases the action takes the form of a standard φ^4-field theory,

$$S = \frac{1}{2} \int d^2 x \sum_{a=1}^{2} (|\partial_\mu z_a|^2 + \mu_a |z_a|^2) + \sum_{a,b=1}^{2} g_{ab} |z_a|^2 |z_b|^2. \tag{5}$$

In Eq. (5) the two modes are in coexistence and interact with each other, but there is no form of chirality and no emerging gauge field as in Eq. (3).

B. Difference between fractionalized PDW and coexistence

We focus on the underdoped cuprate superconductors within the two scenarios mentioned above for the PG [1–3]. However, note that the reality is undoubtedly much more complicated than that due to the proximity to the Mott transition. Nevertheless, here, we restrict ourselves to discuss these two sets of ideas and this simplifies the following analysis enormously.

In the coexistence scenario, a precursor of the SC or the CDW orders forms at T^*. Most of the theories [6,36] that have been advanced so far consider the PDW as a precursor state at T^*. Variational calculations on the t-J model show that the ground state energy of the PDW state is slightly higher than the ground state energy associated with the uniform superconductivity regime [37,38]. Thus, the uniform PDW state is very difficult to stabilize at low temperatures. Some studies [36] suggest that a locally fluctuating PDW state is responsible for opening up a pseudogap in the antinodal regions without ever being the true ground state. At a lower temperature T_{co}, two-dimensional charge modulations do form [39–43] but they have a short-ranged nature. A genuine three-dimensional charge order only forms under an applied magnetic field [42,44,45]. However, at zero fields, the phase of the CDW is fluctuating rapidly in space and this produces a very inhomogeneous density-wave pattern, such as $\chi \cos(\mathbf{Q}_0 \cdot \mathbf{r} + \phi_r)$ with ϕ_r strongly varying from site to site [46–50]. The SC order forms at T_c, leading to the freezing of the SC phase $\Delta \exp(i\theta_{EM})$, due to the usual Meissner effect. The phase gradient gets minimally coupled to the external EM vector potential through a term $n_s(\partial_\mu \theta_{EM} - 2e\mathbf{A})^2$ (where n_s is the superfluid density). Then through a gauge transformation, the vector potential becomes massive, and the SC phase θ_{EM} gets uniform through the sample. However, in the coexistence scenario, even below T_c the CDW order has no mechanism to have a uniform phase and should suffer phase fluctuations from site to site. Hence, for the simple coexistence scenario, the entanglement of the PP and PH pairs is expected to be vanishingly small.

In contrast, in the fractionalization scenario [22–25], the PDW order fails to form at T^*. However, a gauge field (or local phase) emerges, leading to the constraint of Eq. (2). The difference between the two scenarios sets in below T_c, where the two orders coexist. We have now two orders which are related by an emergent gauge field (or, equivalently, by a local phase θ): $\chi \exp(i\theta)$ and $\Delta \exp[i(\theta + \theta_{EM})]$. The local phase θ is minimally coupled to a neutral vector potential through the term $n_\chi(\partial_\mu \theta - e^*\mathbf{a})^2$ (where n_χ is the CDW density and e^* is the fictitious charge). On the other hand, the SC part has a term $n_s(\partial_\mu \theta + \partial_\mu \theta_{EM} - e^*\mathbf{a} - 2e\mathbf{A})^2$. When both orders coexist below T_c both vector potentials $\mathbf{a}$ and $\mathbf{a} + \mathbf{A}$ become massive and are expelled from the sample; in other words, both phases θ and θ_{EM} become uniform, and insensitive to impurities [22]. Effectively the CDW becomes active to the external EM field and behaves as a PDW. In the fractionalization scenario, a strong entanglement thus exists between the PP and PH pairs. Recently a study reported [51] an intriguing observation of a uniform CDW phase inside vortices, and this can be explained by the fractionalized PDW scenario [22]. In this study, we consider another consequence of a
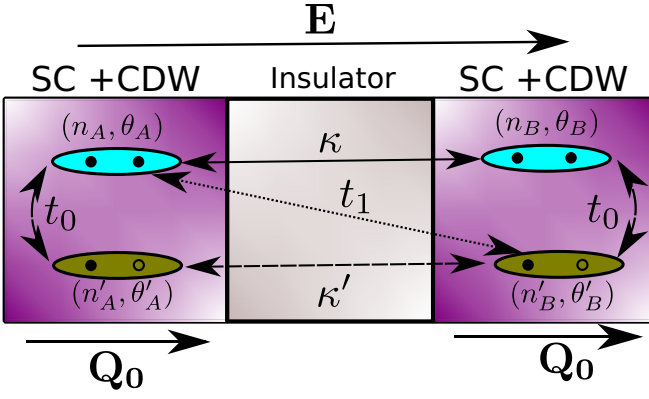
FIG. 1. Josephson junction setup when the applied electric field is parallel to the charge density wave modulation wave vector $\mathbf{Q}_0$. The different possible hoppings between the pairs are presented schematically. κ denotes a PP pair hopping from terminal A to B, and vice versa. κ' represents the same for the hopping of PH pairs across the junction. The interjunction conversion of PP pair to a PH pair is denoted by t_1 and the same within the junction by t_0.

fractionalized PDW, namely, its effects on the current in a Josephson junction setup.

II. MODEL AND METHOD

We propose the experimental setup pictured in Fig. 1. A Josephson junction (JJ) is considered, with underdoped cuprate compounds in two terminals A and B separated by an insulating material. Below T^*, the terminals in A and B access the PG regime and we expect these terminals to display both SC and CDW orders at low temperatures. The JJ is oriented such that the modulation wave vector is parallel to the junction. Moreover, in the present situation, an electric field $\mathbf{E}$ is applied in the same direction as CDW wave vector $\mathbf{Q}_0$.

We consider the following wave functions for the A and B subsystems,

$$|\psi_A\rangle = \sqrt{n_A}e^{i\theta_A} + \sqrt{n'_A}e^{i\theta'_A},$$

$$|\psi_B\rangle = \sqrt{n_B}e^{i\theta_B} + \sqrt{n'_B}e^{i\theta'_B}, \tag{6}$$

where $(n_{A,B}, \theta_{A,B})$ are the superfluid density and phases of SC states on terminals A and B, respectively, and $(n'_{A,B}, \theta'_{A,B})$ are the corresponding CDW density and phases. At a steady state, we take $\theta'_A = \mathbf{Q}_0 \cdot \mathbf{r}$ and $\theta'_B = \mathbf{Q}_0 \cdot (\mathbf{r} + \delta)$. The most generic set of Schrödinger's equations [52,53] that can be written with these two orders, with $\overline{\psi} = (\sqrt{n_A}e^{i\theta_A}, \quad \sqrt{n_B}e^{i\theta_B}, \quad \sqrt{n'_A}e^{i\theta'_A}, \quad \sqrt{n'_B}e^{i\theta'_B})$, is

$$i\hbar\frac{\partial}{\partial t}\psi = \begin{pmatrix} \mu_\Delta & \kappa & t_0 & t_1 \\ \kappa & -\mu_\Delta & t_1 & t_0 \\ t_0 & t_1 & V_A & \kappa' \\ t_1 & t_0 & \kappa' & V_B \end{pmatrix}\psi, \tag{7}$$

where κ and κ' are the hopping integrals for particle-particle (PP) and particle-hole (PH) pairs across the junctions. The parameter $\mu_\Delta = eU$, where U is the electrical potential applied to the PP pairs. In terms of the applied electric field $\mathbf{E}$, this becomes $\mu_\Delta = -e\mathbf{E}r_{A,B}$, where $r_{A,B}$ is the distance with

respect to the center. However, in this study, μ_Δ is assumed to be a constant as in the standard JJ setup [52]. The parameter t_1 represents the tunneling between the PP pairs in the junction A (resp. B) to the modulated PH pairs in junction B (resp. A), whereas t_0 is the same type of tunneling within a junction. The electric field acts on the CDW sector [54] as $V_{A,B} = e E \bar{\rho} \theta'_{A,B}$, where $\bar{\rho} = n'/Q_0$ is an effective CDW density divided by the ordering wave vector $\mathbf{Q}_0$. We have assumed that the superfluid density and the CDW densities are constant throughout the JJ. Although this is not necessary, such assumption simplifies the following analysis enormously. Equations (7) can be decoupled into (for details see Appendix A)

$$\frac{\partial\bar{n}}{\partial t} = \frac{4}{\hbar}\left[-\kappa n \sin\theta + \sqrt{nn'}\cos\frac{\phi}{2}\right.$$
$$\left.\times\left(t_0\sin\frac{\theta'-\theta}{2} - t_1\sin\frac{\theta'+\theta}{2}\right)\right], \tag{8}$$

$$\frac{\partial\theta}{\partial t} = \frac{2}{\hbar}\left[\mu_\Delta + \sqrt{\frac{n'}{n}}\sin\frac{\phi}{2}\right.$$
$$\left.\times\left(t_0\sin\frac{\theta'-\theta}{2} - t_1\sin\frac{\theta+\theta'}{2}\right)\right], \tag{9}$$

$$\frac{\partial\bar{n}'}{\partial t} = \frac{4}{\hbar}\left[-\kappa'n'\sin\theta' + \sqrt{nn'}\cos\frac{\phi}{2}\right.$$
$$\left.\times\left(t_0\sin\frac{\theta-\theta'}{2} - t_1\sin\frac{\theta'+\theta}{2}\right)\right], \tag{10}$$

$$\frac{\partial\theta'}{\partial t} = \frac{1}{\hbar}\left[(V_A - V_B) - 2\sqrt{\frac{n'}{n}}\sin\frac{\phi}{2}\right.$$
$$\left.\times\left(t_0\sin\frac{\theta-\theta'}{2} - t_1\sin\frac{\theta'+\theta}{2}\right)\right], \tag{11}$$

$$\frac{\partial\phi}{\partial t} = -\frac{1}{\hbar}[(V_A + V_B) + 2\kappa\cos\theta + 2\kappa'\cos\theta'$$
$$-\frac{2\delta n}{\sqrt{nn'}}\left(t_0\cos\frac{\theta-\theta'}{2} + t_1\cos\frac{\theta+\theta'}{2}\right)], \tag{12}$$

with $\theta = \theta_B - \theta_A$, $\theta' = \theta'_B - \theta'_A$, $\phi = \theta'_B + \theta'_A - \theta_A - \theta_B$, $\bar{n} = n_B - n_A$, $\bar{n}' = n'_A - n'_B$, $\delta n = n' - n$. Furthermore, we assumed that the density of PP pairs and PH pairs in both terminals are similar, i.e., $n \simeq n_A \simeq n_B$, $n' \simeq n'_A \simeq n'_B$. The variation of ϕ can be simplified further in the limit where $n \simeq n'$, $\delta n \ll n$. In this limit, Eq. (12) simplifies to

$$\frac{\partial\phi}{\partial t} \approx -\frac{1}{\hbar}[(V_A + V_B) + 2\kappa\cos\theta + 2\kappa'\cos\theta']. \tag{13}$$

Next we elucidate on the other parameters. The difference of the electric field on the CDW sector can be simplified to $V_A - V_B = -(eEn'/Q_0)\theta' \equiv -r_0\theta'$, where we have introduced a new parameter $r_0 = eEn'/Q_0$. Similarly, the average potential acting on the CDW sector due to the applied electric field can be treated as constant, i.e., $V_A + V_B = \eta$.

III. RESULTS

In this section we provide the results by solving Eqs. (8)–(13) and finding the Josephson current. First we discuss the terms t_0 and t_1 that generate the main difference between the two scenarios. For the simple coexistence of orders, the

phases of the CDW and SC orders are not linked as discussed in Sec. I B. Therefore, CDW pairs have no mechanism for having a uniform phase over the whole sample. Consequently, it suffers phase shifts and will fluctuate widely from site to site. Such an incoherent CDW pattern is expected to have minimal overlap with the SC pairs. Therefore, we can safely ignore the hopping from a PP pair to a PH pair, as the quantum entanglement between the orders is weak. We can set the parameters $t_0 = \langle \psi_{SC}^{A(B)} | \psi_{CDW}^{A(B)} | \psi_{SC}^{A(B)} | \psi_{CDW}^{A(B)} \rangle = 0$ and $t_1 = \langle \psi_{SC}^{A(B)} | \psi_{CDW}^{B(A)} | \psi_{SC}^{A(B)} | \psi_{CDW}^{B(A)} \rangle = 0$ in Eq. (7) for the coexistence of orders.

In the fractionalized PDW case the CDW phase θ' is such that phase of the two electrodes is given by

$$\theta'_A = \mathbf{Q}_0 \cdot \mathbf{x} + \delta\theta'_A, \quad \theta'_B = \mathbf{Q}_0 \cdot (\mathbf{x} + \delta) + \delta\theta'_B, \quad (14)$$

where δ is a dephasing from electrode A to B. $\delta\theta'_{A(B)}$ are the fluctuations of the phase from the initial steady state. In the setup of Fig. 1 when the electric field and wave vector Q_0 are parallel, δ is controlled by distance between the two electrodes. In Fig. 5(a) we study an independent configuration, where the electric field and Q_0 are perpendicular. In such a case the dephasing is controlled by the initial phase shift of the CDW wave vector in the direction perpendicular to the electrodes. The main difference between the coexisting case is that now θ and θ' are not independent. Since the phase of Δ_{PDW} is coupled to the EM field but has $\mathbf{Q}_0$ modulations as well, we have

$$\theta = \delta\theta' + \theta_{EM}, \quad (15)$$

where θ_{EM} is the electromagnetic phase and $\delta\theta' = \delta\theta_B - \delta\theta_A$. Assuming that we are deep inside the SC phase, with unfractionalized Cooper pairs around, the Meissner effect leads to a uniform EM field [22]. Thus effectively the CDW becomes active to the external EM field, due to the Meissner effect as the phase of the CDW becomes insensitive to the impurities and acts like a PDW order. Therefore a uniform CDW pattern is induced inside the SC phase, an astonishing result that has been reported in scanning tunneling microscopy experiments [51]. Since all the phases are fixed, we now get a finite tunneling t_1 and t_0 back and forth from the modulated CDW and SC phases, and Eqs. (8)–(13) need to be solved with $t, t_0 \neq 0$.

For both scenarios, the usual Josephson current is modified due to the presence of the CDW [52,53], with

$$I_J = -\frac{1}{2}\frac{\partial \bar{n}}{\partial t} - \frac{1}{\pi}\frac{\partial \theta'}{\partial t}. \quad (16)$$

Note that the two fluids couple in the opposite way to the field—the tunneling of the charge two bosons contributes to the conventional SC Josephson current. In contrast, the variation of the phase creates a charge imbalance in the case of the CDW and generates an additional current. We solve Eqs. (8)–(13) and evaluate the Josephson current by using Eq. (16). Since the difference between the two scenarios sets in at T_c, we focus on the zero-temperature limit of the Josephson current. Next we study the alternating current (AC) Josephson effect by applying a constant potential difference between the terminals.

A. AC Josephson effect

1. Coexistence case

For the simple coexistence of orders since the parameters t_0 and t_1 vanish, Eqs. (8)–(13) simplify enormously. Solving for Eq. (16) we get

$$I_J = \frac{2\kappa n}{\hbar}\sin\left(\frac{2\mu_\Delta}{\hbar}t + C_1\right) + \frac{C_2 r_0}{\pi\hbar}e^{-r_0 t}. \quad (17)$$

Here C_1 and C_2 are constants of integration and depend on the initial experimental setup. The first term in Eq. (17) is the standard AC Josephson current with the primary Josephson frequency, $\omega_0 = (2eU)/\hbar$. Similarly, one can define the standard Josephson time period by $T = 2\pi/\omega_0$. The second term arises due to CDW in the situation of coexisting order. Since the SC and CDW orders are disconnected, we only observe a transient response from the CDW phase variation. We have plotted the current I_J as a function of time t in Fig. 2(a) for the coexistence of CDW and SC. The parameters used to obtain Fig. 2(a) are given by $\mu_\Delta = 1.0$, $n = 1.0$, $n' = 1.0$, $r_0 = 3.0$, $\eta = 0.3$, $\kappa = 0.5$, $\kappa' = 0.6$, with $t_1 = t_0 = 0$. We measure all the energies in units of 2κ which we have set to unity. Furthermore, we have also set the constants $e = 1$ and $\hbar = 1$. We have also used the initial conditions $\theta(t = 0) = 0$, $\phi(0) = 0$, and $\theta'(0) = 0.6$. The transient CDW regime near $t = 0$ paves the way to a standard form of the Josephson current for a standard SC current for $t \gg r_0$. In this situation, $I_J(t)$ from the numerical calculations presented in the black dotted trace and the analytical form of Eq. (17) depicted in the red thick trace in Fig. 2(a) match exactly.

2. Fractionalized PDW case

In the fractionalized PDW scenario the terms t_0 and t_1 are nonvanishing. We have obtained an approximate solution of the Josephson current in Appendix B. The Josephson current in the first-order perturbation in t_0 and t_1 is given by

$$\begin{aligned} I_J &= \frac{2\kappa n}{\hbar}\sin\left(\frac{2\mu_\Delta}{\hbar}t + C_1\right) + \frac{C_2 r_0}{\pi\hbar}e^{-r_0 t} \\ &\quad - \frac{2\sqrt{nn'}}{\hbar}\cos\frac{\phi_0}{2}\left(t_0\sin\frac{\theta'_0 - \theta_0}{2} - t_1\sin\frac{\theta'_0 + \theta_0}{2}\right) \\ &\quad + \frac{2}{\pi\hbar}\sqrt{\frac{n'}{n}}\sin\frac{\phi_0}{2}\left(t_0\sin\frac{\theta_0 - \theta'_0}{2} - t_1\sin\frac{\theta_0 + \theta'_0}{2}\right). \end{aligned} \quad (18)$$

The time evolution of zeroth-order ($t_0 = 0$, $t_1 = 0$) solutions of θ_0, θ'_0, and ϕ_0 is given by

$$\theta_0 = \frac{2\mu_\Delta}{\hbar}t + C_1, \quad (19)$$

$$\theta'_0 = \frac{C_2}{\hbar}e^{-r_0 t}, \quad (20)$$

$$\phi_0 = -\frac{\eta}{\hbar}t + C_3 + \frac{2\kappa'}{r_0\hbar}\text{Ci}[C_2 e^{-r_0 t}] - \frac{\kappa}{\mu_\Delta}\sin\left(\frac{2\mu_\Delta}{\hbar}t + C_1\right), \quad (21)$$

where again C_3 is a constant of integration and Ci[x] is the cosine integral function.

We have displayed the current of Eq. (18) in Fig. 2(b) for the same set of parameters as in Fig. 2(a) albeit with a finite
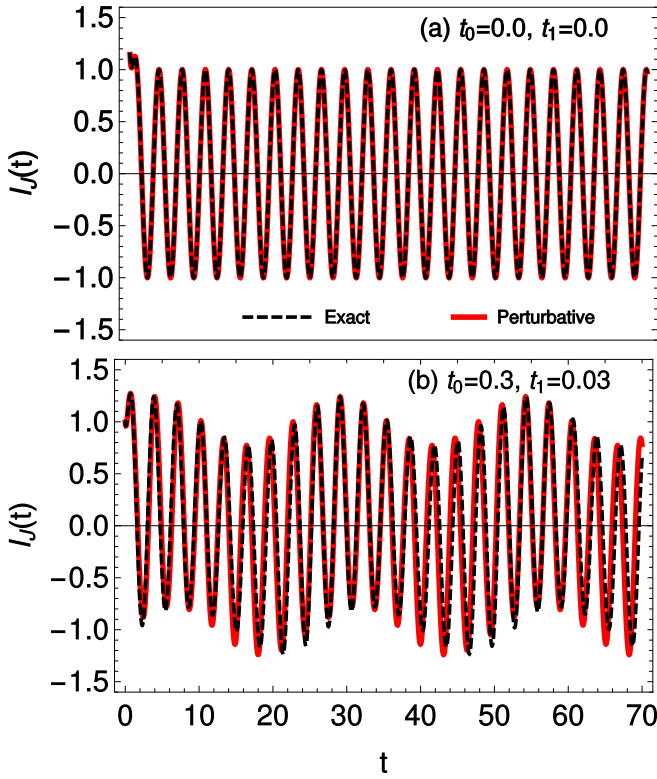
FIG. 2. The variation of Josephson current with time for the setup presented in Fig. 1, i.e., the applied electric field, is parallel to the charge modulation wave vector. Here we compare the exact numerical results with the analytical form of the current calculated perturbatively. Panel (a) shows the situation when the two orders coexist, for a vanishing t_0 and t_1. In this situation, the perturbative calculations are exact. The initial transient current regime for CDW order vanishes at a long-time limit, and we are left with the simple AC Josephson effect. Panel (b) presents the Josephson current for the situation when the entanglement between the orders forms a fractionalized PDW or PDW with a finite $t_0 = 0.3, t_1 = 0.03$. The perturbative calculations and the numerical analysis show a good match. Interestingly, the presence of entanglement between CDW and SC orders induces a beatlike modulation of the Josephson current, which can be contrasted with the simple coexistence scenario presented above.

$t_0 = 0.3, t_1 = 0.03$. The perturbative analytical calculations match well with the exact numerical form of the current. The Josephson current for the fractionalized PDW displays a beatlike structure which is strikingly distinguishable from the coexistence case. This provides us with the first prediction: If the PG phase of the underdoped cuprates supports a PDW or fractionalized PDW state, the AC Josephson current should develop a beatlike form as shown in Fig. 2(b), whereas if the orders simply coexist in the PG phase the AC Josephson current in long times will follow the conventional form.

3. Frequency of the AC Josephson current

The Josephson current for a fractionalized PDW state shows a beatlike structure that suggests multiple frequencies contribute to the AC Josephson current. To get the frequency,

we need to perform a Fourier transform of the AC Josephson current to the frequency domain.

We simplify the Eq. (18) by assuming that the interjunction PP to PH hopping amplitude is small compared to the intra-junction hoppings, i.e., $t_1 \ll t_0$. In an experimental scenario, this requires using a barrier to decay the PH hoppings across the junction. However, for a finite but small t_1, will not create any qualitative difference to the discussion below. Also, in the long-time limit, the transient current regime from the CDW vanishes, i.e., $\theta_0' \to 0$. Following the manipulations detailed in Appendix C, we obtain

$$
\begin{aligned}
I_J \approx \frac{t_0 \sqrt{nn'}}{\hbar} &(\mathcal{J}_0(b)(\sin a_+ t + \sin a_- t) \\
&+ \mathcal{J}_1(b)\{\sin[(a_+ + \xi)t] - \sin[(a_- + \xi)t] \\
&+ \sin a_- t - \sin a_+ t\}) + \frac{2\kappa n}{\hbar} \sin \xi t,
\end{aligned} \tag{22}
$$

where $\mathcal{J}_\nu(x)$ is the Bessel function of first kind of the νth order. Also we have redefined

$$
a_\pm = \frac{1}{2}\left(\frac{2\mu_\Delta}{\hbar} \pm \frac{\eta}{\hbar} \pm \frac{2\kappa'}{\hbar} \right), \tag{23}
$$

$$
b = \frac{\kappa}{2\mu_\Delta}, \tag{24}
$$

$$
\xi = \frac{2\mu_\Delta}{\hbar}. \tag{25}
$$

Since all the terms are directly proportional to t, one can easily read off the frequencies for the AC current, by performing a Fourier transform. This is given by

$$
\begin{aligned}
\tilde{I}_J(\omega) = \frac{\kappa n}{\hbar} \delta(\omega - \xi) + \frac{t_0 \sqrt{nn'}}{2\hbar} &\{[\mathcal{J}_0(b) + \mathcal{J}_1(b)]\delta(\omega - a_-) \\
&+ \mathcal{J}_1(b)\delta(\omega - a_+ - \xi) - \mathcal{J}_1(b)\delta(\omega - a_- - \xi) \\
&+ [\mathcal{J}_0(b) - \mathcal{J}_1(b)]\delta(\omega - a_-)\}.
\end{aligned} \tag{26}
$$

The primary frequency ξ is the usual AC Josephson frequency. The other frequencies are the additional ones originating due to the entanglement of the two orders. The ratio of the primary to the few additional frequencies is given by

$$
\frac{\omega_1}{\omega_0} = \frac{1}{2} - \left(\frac{\eta + 2\kappa'}{4eU} \right), \tag{27}
$$

$$
\frac{\omega_4}{\omega_0} = \frac{1}{2} + \left(\frac{\eta + 2\kappa'}{4eU} \right), \tag{28}
$$

$$
\frac{\omega_2}{\omega_0} = \frac{3}{2} + \left(\frac{\eta + 2\kappa'}{4eU} \right), \tag{29}
$$

$$
\frac{\omega_3}{\omega_0} = \frac{3}{2} - \left(\frac{\eta + 2\kappa'}{4eU} \right), \tag{30}
$$

where ω_{i-1} are the ith delta-function peak of Eq. (26) and we used the fact that $\mu_\Delta = eU$, where U is the DC potential applied across the terminals. For large potential difference between the two junctions, i.e., $U \gg \eta + 2\kappa'$, the second term of all the ratios vanishes. Moreover, the ratio between the primary and additional frequencies will occur at half-odd integers, i.e., $1/2, 3/2, 5/2, \ldots$. However, the peak intensity will diminish for the higher-order peaks as the higher-order Bessel functions determine their strength.
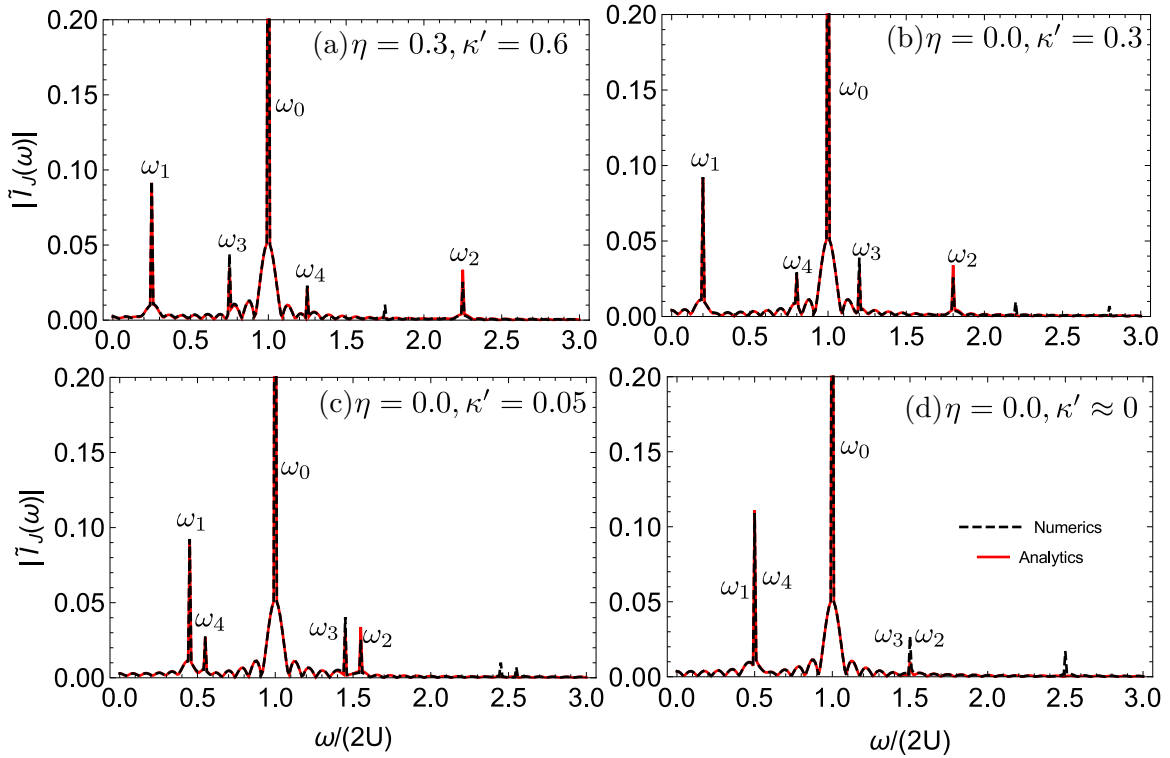
FIG. 3. Exhibits the primary ω_0 and additional frequencies ω_i of AC Josephson current for $t_0 = 0.3$, $t_1 = 0.0$. Here κ' and η are material-dependent parameters. As the potential difference between the two terminals dominates the material-dependent parameters, the number of peaks reduces due to the merging of peaks as shown in (c) and (d). The additional peaks for $U \gg \eta + 2\kappa'$ are at the half-odd integer multiples of the primary peak ω_0.

We have presented in Fig. 3 the Fourier transform of the Josephson current given in Eq. (18) solved numerically compared with the perturbative solution of Eq. (26). The dominant peaks of the AC Josephson junction are captured within our approximate analysis. The primary peak ω_0 arising from the normal AC Josephson effect remains unchanged for all the parameters. In Figs. 3(a) and 3(b) when $U \sim \eta + 2\kappa'$, the four additional peaks are separated and well resolved. The separation of the peaks ω_1 and ω_4 from $0.5\omega_0$ (similarly ω_2 and ω_3 from $1.5\omega_0$) should reduce monotonically as the potential difference between the two electrodes increases. This is illustrated in Figs. 3(b) to 3(d). When $U \gg \eta + 2\kappa'$, the two peaks merge as shown in Figs. 3(c) and 3(d) which leads to an apparent reduction in the number of peaks. Therefore when the potential difference between the terminals is large compared to the material-dependent parameters, the additional frequencies occur at half-odd integers of ω_0. Studying such frequency dependence of the AC Josephson current peaks will give strong evidence for the fractionalized PDW scenario.

4. Envelope of the AC Josephson current

We have also obtained the envelope for the oscillation observed for the fractionalized PDW situation. The details for obtaining the same are presented in Appendix D. To do this we performed a few simplifications. First, we assume that the interjunction PP to PH hopping amplitude is small compared to the intrajunction hoppings, i.e., $t_1 \ll t_0$. This is not necessary *a priori* but it simplifies the following discussion. Experimen-

tally, this requires hindering the t_1 hopping by using a suitable barrier. Second, since the envelope exists even in the long-time limit the transient response can be safely ignored. Third, the expressions of current are first-order perturbative solutions in t_0. We find that the expression for the current in this limit becomes

$$I_J \approx \frac{n}{\hbar} \Big[\sqrt{\kappa^2 + t_0^2 + 2\kappa t_0 \cos \chi_1}$$
$$+ \sqrt{\kappa^2 + t_0^2 + 2\kappa t_0 \cos \chi_2} \Big] \sin(\theta_0), \qquad (31)$$

where $\chi_1 = (\phi_0 - \theta_0)/2$ and $\chi_2 = (\phi_0 + \theta_0)/2$.

The total envelope is shown by the red trace in Figs. 4(a) and 4(b) which is the term inside the square brackets in Eq. (31). The envelope term which captures the slower oscillation is exhibited by the blue traces in Fig. 4. We note that this is controlled by the χ_1 term. Additionally, the beatlike oscillations for the fractionalized PDW become better resolved as the entanglement between the two orders increases. Experimental observation of such dependence will also signal the fractionalized PDW in the pseudogapped phase of the underdoped cuprates.

5. Extracting modulation wave vector

It is also possible to detect the PDW modulation wave vector by varying the dephasing parameter δ between the two electrodes and by investigating its effect on the average Josephson current. The initial phases for the particle-hole pairs are given in Eq. (14), $\theta' = Q_0\delta$ and $\phi = Q_0\delta + \gamma$, where
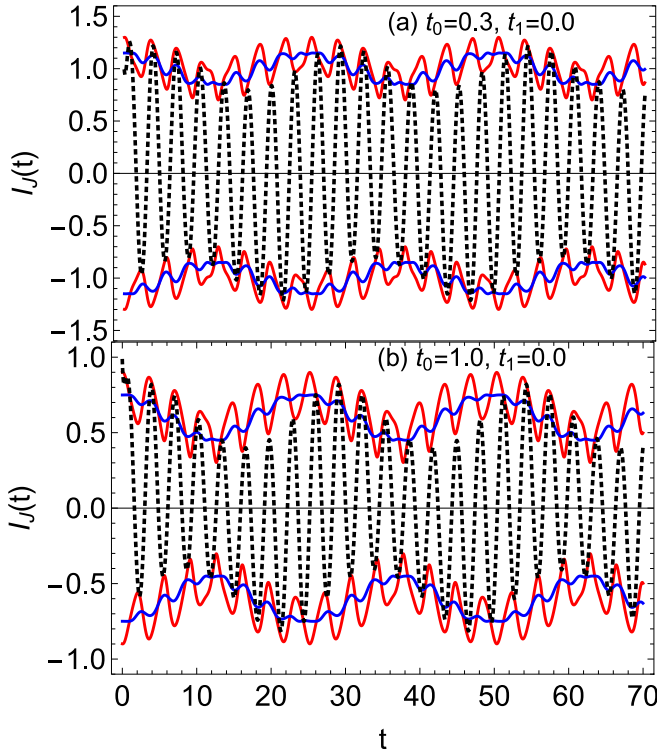
FIG. 4. Presents the evolution of the beatlike form of the Josephson current for two different parameters (a) $t_0 = 0.3$, (b) $t_0 = 1$. The total envelope for the oscillation is governed by the red traces, which still contain some modulations. The blue trace shows the slower oscillation of the envelope which is controlled by the first term of Eq. (31) and hence by $\chi_1 = (\phi_0 - \theta_0)/2$. This additional oscillation of the envelope is due to the entanglement between the SC and CDW order.

FIG. 5. Panel (a) depicts the variation of average Josephson current with the width of the insulating region, δ. The current shows a linear increase for a simple coexistence of two orders, with the slope proportional to the CDW modulation wave vector. However, for a fractionalized PDW state, the Josephson current reveals a weak modulation with δ. Panel (b) shows the derivative of the current presented in panel (a). The PDW modulation wave vector $\mathbf{Q_0}$ controls the oscillation of the Josephson current with δ, albeit higher harmonics of oscillations are also present.

γ can be set to a constant. Similarly, the phase difference for the particle-particle pairs, $\theta = C_1$, is also a constant at $t = 0$, which depends on the initial condition of the JJ setup.

We average the Josephson current, $\langle I_J \rangle$, using Eq. (18) over a time of 10% of the primary Josephson period T. For the coexistence of order the $\langle I_J \rangle$ is presented in Fig. 5(a) in the red trace for $r_0 = 1.2$, $C_1 = 0$, and $Q_0 = (1/4)2\pi/a_0$, where a_0 is the lattice spacing set to unity. The expression is linearly increasing with the width of the junction. The slope of the linear increase is proportional to the modulation wave vector Q_0.

However, for the fractionalized PDW scenario, along with the linear increase of the current with δ, there is also weak oscillation as shown in the black trace in Fig. 5(a). The modulation can be better identified by the derivative of $\langle I_J \rangle$ with respect to δ. We depicted the same in Fig. 5(b), and it shows oscillations with the primary wavelength of $2\pi/Q_0$. However, higher moments of oscillations make it challenging to determine the magnitude of the PDW wave vector (for details, see Appendix E 1). We also note that such Josephson junction is difficult to set up in practice. In this setup, the width of the insulating region increases, which should also modify the interjunction hopping for different δ. Moreover, fabricating JJ with varying sizes of the insulating region is challenging.
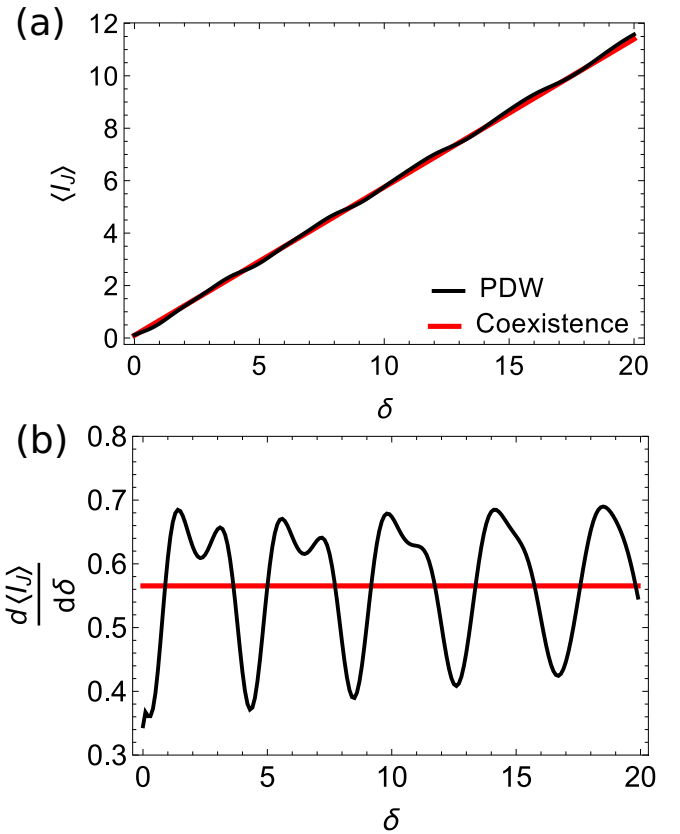
Next, we discuss another complementary Josephson junction setup better suited to extracting the modulation wave vector Q_0. Figure 6(a) shows a JJ setup where the modulation wave vector is perpendicular to the electric field. Here δ denotes the phase shift of the CDW wave vector in the B electrode with respect to the A. In this situation, V_A and V_B vanish and hence $r_0 = \eta = 0$. In Fig. 6(b) we plot the variation average Josephson current with δ, time-averaged over 0.1 of the usual SC Josephson period. The details of the calculations are presented in Appendix E 2. Here, the fractionalized PDW scenario displays modulation controlled by $2\pi/Q_0$. In contrast, the coexistence scenario gives a flat average current with varying δ. In Fig. 6(c), we also establish that the modulation of the I_J with δ remains robust when time averaging is done over 20% of the primary Josephson period. Therefore, in this setup, it should be possible to extract the modulation wave vector of the PDW.

B. Inverse Josephson effect

In the previous section, we used a constant DC voltage U across the junction, leading to an AC Josephson current. It is
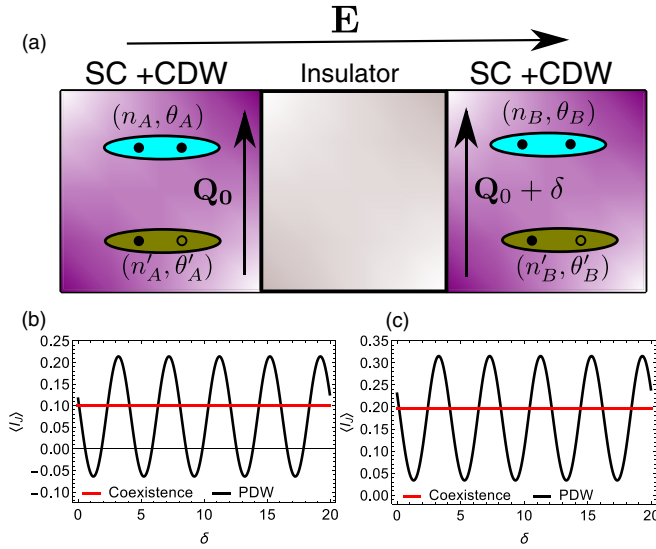
(a)

(b)

(c)

FIG. 6. Panel (a) shows a Josephson junction setup in which the electric field is perpendicular to the charge modulation wave vector. The CDW modulations in the two terminals are dephased by a factor of δ here. Panel (b) depicts the evolution of the average Josephson current with the dephasing parameter δ. Here the $\langle I_J \rangle$ is time-averaged over 10% of the primary Josephson period. For the coexistence of orders, the average current with the dephasing parameter is constant. However, for the fractionalized PDW scenario, the Josephson current modulates with the modulation proportional to the CDW wave vector $\mathbf{Q}_0$. (c) The same as (b) but averaged over 20% of the primary Josephson period.

also possible to apply a microwave AC voltage to the junction, such that $U(t) = U + \tilde{U} \cos \omega t$. Here U is the constant DC voltage. Note that we have used an insulating barrier, so the normal current passing through the junction will vanish. Solving for the Josephson current, for the simple coexistence of orders, the Josephson current is given by

$$I_J = \frac{2\kappa n}{\hbar} \sum_{m=-\infty}^{\infty} \left[(-1)^m \sin \left(C_1 + \frac{2eU}{\hbar} t - m\omega t \right) \right.$$
$$\left. \times \mathcal{J}_m \left(\frac{2e\tilde{U}}{\hbar \omega} \right) \right] + \frac{C_2 r_0}{\pi \hbar} e^{-r_0 t}, \quad (32)$$

where m is an integer and $\mathcal{J}_m$ is the Bessel function of the first kind of order m. The time average of this quantity gives the DC current I_{DC}. The long-time average of the oscillatory term vanishes unless the frequency ω is some integral multiple of the applied DC voltage U in the units where we set $(2e)/\hbar = 1$. The transient current also fades away in the long-time limit. The DC current in that scenario is given by

$$|I_{DC}| \approx \frac{2\kappa n}{\hbar} \sum_{m=-\infty}^{\infty} \delta_{m\omega,U} (-1)^m \mathcal{J}_m \left(\frac{\tilde{U}}{\omega} \right) \sin C_1, \quad (33)$$

which leads to sharp δ peaks at the integer multiples of the AC frequency ω. These peaks are known as Shapiro spikes. We have presented the details of Shapiro spikes in Appendix H.

Usually, in experiments, the circuit is driven by current instead of voltage. The nature of current versus voltage characteristics can be qualitatively explained from the Shapiro
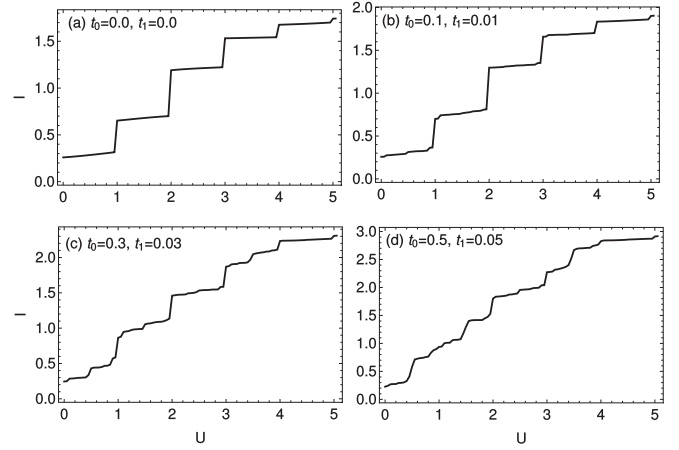

FIG. 7. Demonstration of the current-voltage characteristics in the inverse Josephson setup. In (a) we set $t_0 = 0, t_1 = 0$ the parameter corresponding to the simple coexistence of CDW and SC orders. The sharp Shapiro steps can be observed when the applied DC voltage U is equal to the integer multiple of the frequency ω. In (b)–(d) we plot the same for finite t_0, t_1 which corresponds to the fractionalized PDW scenario. In (b) t_0, t_1 is small, and other steps start developing in between the two steps. In (c) and (d) these additional steps become stronger as the entanglement between the two orders is increased and some of the integer steps vanish completely.

spikes. For instance, when the external driven current exceeds the strength of the Shapiro spike at some voltage, the voltage increases abruptly with almost zero slopes until the voltage reaches the next spike. In the subsequent level, again, as the current increases to that of the spike strength, the voltage remains stable. As the current exceeds the spike strength, the voltage again shoots up until the next spike is reached. This pattern keeps repeating itself, creating a steplike current-voltage characteristic known as Shapiro steps.

We have solved Eqs. (8)–(13) for an AC voltage of the form $U(t) = U + \tilde{U} \cos \omega t$ and plotted the DC current as a function of the U in the units where we set $(2e)/\hbar = 1$ in Fig. 7. In all these figures we have used the parameters same as in Fig. 2 with AC frequency $\omega = 1$ and AC voltage amplitude $\tilde{U} = 3.0, C_1 = \pi/2$. We have presented the predicted current-driven nature of the current-voltage characteristics in Fig. 7. For the coexistence case, $t_0, t_1 = 0$ and we find in Fig. 7(a) the expected sharp Shapiro steps at the integer multiples of ω.

Next, we solve Eqs. (8)–(13) numerically for an AC voltage of the same form but a finite t_0, t_1 and track the evolution of the Shapiro steps. In Fig. 7(b) we present the results for $t_0 = 0.1, t_1 = 0.01$, i.e., a small entanglement between the two orders leading to a weak PDW state. We find that the Shapiro steps become broader as soon as the entanglement between the two orders is turned on. New steps start to appear as the overlap between the charge and SC order increases in Fig. 7(c). Finally, for a strong entanglement between the two orders, some steps appear at different DC voltage than the integer multiples of ω. Interestingly, in Fig. 7(d), the first integer Shapiro step at $U = 1$ is thoroughly washed away as new steplike feature forms at $U = 1/2$. Therefore, our calculations suggest that additional fractional Shapiro steps in the inverse Josephson junction setup will strongly favor the PDW

scenario. However, the conventional nature of voltage-current characteristics will manifest for a competing order scenario.

IV. SUMMARY AND CONCLUSIONS

We propose a Josephson junction setup that can distinguish between two possible scenarios which can be observed in the enigmatic pseudogap phase of the cuprates. We focused on the case of a fractionalized PDW state which can turn into interconverted SC and CDW pairs and compare this with the scenario where the SC and the CDW orders simply coexist with each other. Our findings are that in the case of a fractionalized PDW phase,

(i) we observe a beatlike structure of AC Josephson current when a constant DC voltage is applied across the junction;

(ii) the additional frequencies for the AC Josephson current are at the half-odd integer multiples of the normal Josephson frequency for a large value of constant DC voltage;

(iii) we can detect modulations of the Josephson current with a period proportional to the CDW wave vector $\mathbf{Q}_0$ by varying the dephasing parameter of the CDW modulation in two terminals;

(iv) in the inverse Josephson setup, the induced DC current has additional steps other than the standard integer Shapiro steps.

Identification of these signatures will strongly indicate the fractionalized PDW scenario for the pseudogap phase. Recently signatures of PDW order are seen in $Bi_2Sr_2CaCu_2O_{8+x}$ using a Josephson scanning tunneling microscopy setup [11,26]. We therefore expect to observe these effects on such materials. Moreover, the predictions presented here are not dependent on the fine-tuning of material-dependent parameters.

We note that the Josephson junction setup is shown in Fig. 1 and Fig. 6(a) presents just the two representative cases. For instance, in Fig. 1, the applied electric field is parallel to the modulation wave vector and in Fig. 6(a), the modulation wave vector is perpendicular to the applied field. However, only short-ranged domains of unidirectional modulations are observed in cuprates [55]. Therefore, the samples in both terminals can contain an admixture of unidirectional domains of modulated orders. Importantly, our analysis shows that the presence of one scenario cannot critically affect the other. Consequently, we expect to discern a superposition of these two effects presented in this paper.

Recent studies have used Josephson scanning tunneling microscopy to observe the modulation of the Josephson current [11,26]. In such studies, both the tip and sample are in the underdoped regime of the cuprates. The tips have been fabricated from the flakes of the sample itself, leading to the possible detection of the pair density wave states in cuprates. If the wave vectors of both the tip and sample align perpendicular to the applied field, the situation of Fig. 6(a) will manifest. As the tip is moved parallel over the sample, it changes the dephasing parameter δ. The Josephson current modulates with the wave vector $\mathbf{Q}_0$ as a function of δ [11,26], very similar to our observation in Fig. 6.

Our calculations provide several predictions of the Josephson setups to detect PDW states. Any experiments that can test these features will be instrumental in differentiating between the simple coexistence of orders and the proposed pair density wave scenario.

APPENDIX A: THE SCHRÖDINGER EQUATIONS

In this section we provide complementary details on how to derive Eq. (7). We rewrite Eq. (7) as

$$i\hbar\frac{\partial}{\partial t}(\sqrt{n_A}e^{i\theta_A}) = \mu_\Delta\sqrt{n_A}e^{i\theta_A} + \kappa\sqrt{n_B}e^{i\theta_B}$$
$$+ t_0\sqrt{n'_A}e^{i\theta'_A} + t_1\sqrt{n'_A}e^{i\theta'_B}, \quad (A1)$$

$$i\hbar\frac{\partial}{\partial t}(\sqrt{n_B}e^{i\theta_B}) = -\mu_\Delta\sqrt{n_B}e^{i\theta_B} + \kappa\sqrt{n_A}e^{i\theta_A}$$
$$+ t_0\sqrt{n'_B}e^{i\theta'_B} + t_1\sqrt{n'_A}e^{i\theta'_A}, \quad (A2)$$

$$i\hbar\frac{\partial}{\partial t}(\sqrt{n'_A}e^{i\theta'_A}) = V_A\sqrt{n'_A}e^{i\theta'_A} + \kappa'\sqrt{n'_B}e^{i\theta'_B}$$
$$+ t_0\sqrt{n_A}e^{i\theta_A} + t_1\sqrt{n_B}e^{i\theta_B}, \quad (A3)$$

$$i\hbar\frac{\partial}{\partial t}(\sqrt{n'_B}e^{i\theta'_B}) = V_B\sqrt{n'_B}e^{i\theta'_B} + \kappa'\sqrt{n'_A}e^{i\theta'_A}$$
$$+ t_0\sqrt{n_B}e^{i\theta_B} + t_1\sqrt{n_A}e^{i\theta_A}. \quad (A4)$$

Expanding Eq. (A1) and taking the complex conjugate of it yields

$$i\hbar(\dot{\sqrt{n_A}} + i\dot{\theta}_A\sqrt{n_A})e^{i\theta_A} = \mu_\Delta\sqrt{n_A}e^{i\theta_A} + \kappa\sqrt{n_B}e^{i\theta_B}$$
$$+ t_0\sqrt{n'_A}e^{i\theta'_A} + t_1\sqrt{n'_A}e^{i\theta'_B}, \quad (A5)$$

$$-i\hbar(\dot{\sqrt{n_A}} - i\dot{\theta}_A\sqrt{n_A})e^{-i\theta_A} = \mu_\Delta\sqrt{n_A}e^{-i\theta_A} + \kappa\sqrt{n_B}e^{-i\theta_B}$$
$$+ t_0\sqrt{n'_A}e^{-i\theta'_A} + t_1\sqrt{n'_A}e^{-i\theta'_B}. \quad (A6)$$

Adding Eqs. (A5) and (A6) leads to

$$\frac{\partial n_A}{\partial t} = \frac{2}{\hbar}[\kappa\sqrt{n_A n_B}\sin\theta + t_0\sqrt{n_A n'_A}\sin(\theta'_A - \theta_A)$$
$$+ t_1\sqrt{n'_B n_A}\sin(\theta'_B - \theta_A)], \quad (A7)$$

where $\theta = \theta_B - \theta_A$. Next subtracting Eq. (A5) from Eq. (A6) leads to

$$\frac{\partial\theta_A}{\partial t} = -\frac{1}{\hbar}\left[\mu_\Delta + \kappa\sqrt{\frac{n_B}{n_A}}\cos\theta + t_0\sqrt{\frac{n'_A}{n_A}}\cos(\theta'_A - \theta_A)\right.$$
$$\left. + t_1\sqrt{\frac{n'_B}{n_A}}\cos(\theta'_B - \theta_A)\right]. \quad (A8)$$

Next repeating the same procedure for Eq. (A2), we obtain the corresponding equations for n_B and θ_B as follows,

$$\frac{\partial n_B}{\partial t} = \frac{2}{\hbar}[-\kappa\sqrt{n_A n_B}\sin\theta + t_0\sqrt{n_B n_B'}\sin(\theta_B' - \theta_B)$$
$$+ t_1\sqrt{n_A' n_B}\sin(\theta_A' - \theta_B)], \qquad (A9)$$

$$\frac{\partial\theta_B}{\partial t} = \frac{1}{\hbar}\left[\mu_\Delta - \kappa\sqrt{\frac{n_A}{n_B}}\cos\theta - t_0\sqrt{\frac{n_B'}{n_B}}\cos(\theta_B' - \theta_B)\right.$$
$$\left. - t_1\sqrt{\frac{n_A'}{n_B}}\cos(\theta_A' - \theta_B)\right]. \qquad (A10)$$

We define $\bar{n} = n_B - n_A$, subtracting Eq. (A7) from Eq. (A9), leading to

$$\frac{\partial\bar{n}}{\partial t} = \frac{2}{\hbar}\{-2\kappa\sqrt{n_A n_B}\sin\theta$$
$$+ t_0[\sqrt{n_B n_B'}\sin(\theta_B' - \theta_B) - \sqrt{n_A n_A'}\sin(\theta_A' - \theta_A)]$$
$$+ t_1[\sqrt{n_A' n_B}\sin(\theta_A' - \theta_B) - \sqrt{n_B' n_A}\sin(\theta_B' - \theta_A)]\}. \qquad (A11)$$

Approximating that the density of particle-particle pairs and particle-hole pairs in both the terminals is similar in the steady state, i.e., $n_A \approx n_B = n$ and $n_A' \approx n_B' = n'$, and defining $\phi = \theta_A' + \theta_B' - \theta_A - \theta_B$, we obtain

$$\frac{\partial\bar{n}}{\partial t} = \frac{4}{\hbar}\left[-\kappa n\sin\theta + \sqrt{nn'}\cos\frac{\phi}{2}\right.$$
$$\left.\times\left(t_0\sin\frac{\theta' - \theta}{2} - t_1\sin\frac{\theta' + \theta}{2}\right)\right], \qquad (A12)$$

where $\theta' = \theta_B' - \theta_A'$. Following the same procedure and approximation we can obtain the differential equation for θ, which is given by

$$\frac{\partial\theta}{\partial t} = \frac{2}{\hbar}\left[\mu_\Delta + \sqrt{\frac{n'}{n}}\sin\frac{\phi}{2}\right.$$
$$\left.\times\left(t_0\sin\frac{\theta' - \theta}{2} - t_1\sin\frac{\theta + \theta'}{2}\right)\right]. \qquad (A13)$$

Repeating the procedure for Eqs. (A3) and (A4), we obtain the differential equation for $\bar{n}'$ and θ':

$$\frac{\partial\bar{n}'}{\partial t} = \frac{4}{\hbar}\left[-\kappa' n'\sin\theta' + \sqrt{nn'}\cos\frac{\phi}{2}\right.$$
$$\left.\times\left(t_0\sin\frac{\theta - \theta'}{2} - t_1\sin\frac{\theta' + \theta}{2}\right)\right], \qquad (A14)$$

$$\frac{\partial\theta'}{\partial t} = \frac{1}{\hbar}\left[(V_A - V_B) - 2\sqrt{\frac{n'}{n}}\sin\frac{\phi}{2}\right.$$
$$\left.\times\left(t_0\sin\frac{\theta - \theta'}{2} - t_1\sin\frac{\theta' + \theta}{2}\right)\right]. \qquad (A15)$$

Using all these forms for the θ's we can obtain the time evolution equation for ϕ:

$$\frac{\partial\phi}{\partial t} = -\frac{1}{\hbar}\left[(V_A + V_B) + 2\kappa\cos\theta + 2\kappa'\cos\theta'\right.$$
$$\left. - \frac{2(n - n')}{\sqrt{nn'}}\left(t_0\cos\frac{\theta - \theta'}{2} + t_1\cos\frac{\theta + \theta'}{2}\right)\right]. \qquad (A16)$$

The fourth term on the right-hand side can be approximately taken to be small when the particle-particle pairs and the particle-hole pairs are of similar strength, i.e., $\delta n/n \ll 1$, and thus we obtain

$$\frac{\partial\phi}{\partial t} \approx -\frac{1}{\hbar}[(V_A + V_B) + 2\kappa\cos\theta + 2\kappa'\cos\theta']. \qquad (A17)$$

We need to solve the five coupled differential equations (A12), (A13), (A14), (A15), and (A17).

APPENDIX B: EVALUATION OF JOSEPHSON CURRENT

The Josephson current is obtained by the expression [52,53]

$$I_J = -\frac{1}{2}\frac{\partial\bar{n}}{\partial t} - \frac{1}{\pi}\frac{\partial\theta'}{\partial t}. \qquad (B1)$$

To find this, we need a solution to the equations presented in the previous section, using the forms for the difference of potential between the two terminals due to charge density modulations as $V_A - V_B = -e\bar{\rho}\theta' \equiv -r_0\theta'$, with the average of the same $V_A + V_B = \eta$ set to constant. The coupled differential equations can be written in a condensed form as

$$\frac{\partial\bar{n}}{\partial t} = \frac{4}{\hbar}\left[-\kappa n\sin\theta + \sqrt{nn'}\cos\frac{\phi}{2}f(t_0, t_1, \theta, \theta')\right], \qquad (B2)$$

$$\frac{\partial\theta}{\partial t} = \frac{2}{\hbar}\left[\mu_\Delta + \sqrt{\frac{n'}{n}}\sin\frac{\phi}{2}f(t_0, t_1, \theta, \theta')\right], \qquad (B3)$$

$$\frac{\partial\bar{n}'}{\partial t} = \frac{4}{\hbar}\left[-\kappa' n'\sin\theta' + \sqrt{nn'}\cos\frac{\phi}{2}g(t_0, t_1, \theta, \theta')\right], \qquad (B4)$$

$$\frac{\partial\theta'}{\partial t} = \frac{1}{\hbar}\left[-r_0\theta' - 2\sqrt{\frac{n'}{n}}\sin\frac{\phi}{2}g(t_0, t_1, \theta, \theta')\right], \qquad (B5)$$

$$\frac{\partial\phi}{\partial t} = -\frac{1}{\hbar}[\eta + 2\kappa\cos\theta + 2\kappa'\cos\theta']. \qquad (B6)$$

Here we have defined

$$f(t_0, t_1, \theta, \theta') = \left(t_0\sin\frac{\theta' - \theta}{2} - t_1\sin\frac{\theta' + \theta}{2}\right), \qquad (B7)$$

$$g(t_0, t_1, \theta, \theta') = \left(t_0\sin\frac{\theta - \theta'}{2} - t_1\sin\frac{\theta + \theta'}{2}\right). \qquad (B8)$$

These equations can be solved using numerical means for any parameter, and the Josephson current can be evaluated using Eq. (B1). However, here we discuss an approach to calculate when the t_0 and t_1 are small parameters that can be incorporated perturbatively in the expression. In this approach, we expand the solutions

$$\bar{n} = \bar{n}_0 + (t_0 + t_1)\bar{n}_1 + (t_0 + t_1)^2\bar{n}_2 + \cdots, \qquad (B9)$$

$$\theta' = \theta_0' + (t_0 + t_1)\theta_1' + (t_0 + t_1)^2\theta_2' + \cdots, \qquad (B10)$$

and so on for other variables, and the subscript represents the perturbative order of the solution. The zeroth-order solution is readily obtained by putting $t_0 = 0$ and $t_1 = 0$ in Eq. (B2) to Eq. (B6). The relevant equations become

$$\frac{\partial \bar{n}_0}{\partial t} = -\frac{4\kappa n}{\hbar} \sin \theta_0, \tag{B11}$$

$$\frac{\partial \theta_0}{\partial t} = \frac{2\mu_\Delta}{\hbar}, \tag{B12}$$

$$\frac{\partial \theta_0'}{\partial t} = -\frac{r_0}{\hbar} \theta_0', \tag{B13}$$

$$\frac{\partial \phi_0}{\partial t} = -\frac{1}{\hbar}[\eta + 2\kappa \cos \theta_0 + 2\kappa' \cos \theta_0']. \tag{B14}$$

The solutions for these equations are readily obtained and these are given by

$$\theta_0 = \frac{2\mu_\Delta}{\hbar} t + C_1, \tag{B15}$$

$$\theta_0' = \frac{C_2}{\hbar} e^{-r_0 t}, \tag{B16}$$

and the zeroth-order Josephson current becomes

$$I_J^{(0)} = \frac{2\kappa n}{\hbar} \sin \left(\frac{2\mu_\Delta}{\hbar} t + C_1 \right) + \frac{C_2 r_0}{\pi \hbar} e^{-r_0 t}, \tag{B17}$$

where C_1 and C_2 are the constants of integration. Notice that the first term is the usual Josephson current for a superconducting junction, whereas the second term is a transient current due to the presence of charge orders. When the entanglement between the orders is small, i.e., for a simple coexistence of order, Eq. (B17) gives the exact form of the current.

Next we focus on obtaining the first-order correction to this current. To this end, we need the zeroth-order expression for ϕ_0, which can be obtained by using θ_0 and θ_0' in Eq. (B14),

$$\phi_0 = -\frac{\eta}{\hbar} t + C_3 + \frac{2\kappa'}{r_0 \hbar} \text{Ci}[C_2 e^{-r_0 t}] - \frac{\kappa}{\mu_\Delta} \sin \left(\frac{2\mu_\Delta}{\hbar} t + C_1 \right), \tag{B18}$$

where again C_3 is a constant of integration and Ci[x] is the cosine integral function. The first-order equations can now be evaluated by taking the derivative of Eq. (B2) and Eq. (B5) with respect to t_0 and t_1 individually and subsequently setting these small parameters to zero. Therefore the first-order correction for the terms relevant for the Josephson current thus becomes

$$\frac{\partial \bar{n}_1}{\partial t} = \frac{4\sqrt{nn'}}{\hbar} \cos \frac{\phi_0}{2} \left(t_0 \sin \frac{\theta_0' - \theta_0}{2} - t_1 \sin \frac{\theta_0' + \theta_0}{2} \right), \tag{B19}$$

$$\frac{\partial \theta_1'}{\partial t} = -\frac{2}{\hbar} \sqrt{\frac{n'}{n}} \sin \frac{\phi_0}{2} \left(t_0 \sin \frac{\theta - \theta_0'}{2} - t_1 \sin \frac{\theta_0 + \theta_0'}{2} \right). \tag{B20}$$

Therefore up to the first order the Josephson current is given by

$$I_J = \frac{2\kappa n}{\hbar} \sin \left(\frac{2\mu_\Delta}{\hbar} t + C_1 \right) + \frac{C_2 r_0}{\pi \hbar} e^{-r_0 t}$$
$$- \frac{2\sqrt{nn'}}{\hbar} \cos \frac{\phi_0}{2} \left(t_0 \sin \frac{\theta_0' - \theta_0}{2} - t_1 \sin \frac{\theta_0' + \theta_0}{2} \right)$$
$$+ \frac{2}{\pi \hbar} \sqrt{\frac{n'}{n}} \sin \frac{\phi_0}{2} \left(t_0 \sin \frac{\theta_0 - \theta_0'}{2} - t_1 \sin \frac{\theta_0 + \theta_0'}{2} \right), \tag{B21}$$

where we can use the time evolution of θ_0, θ_0', and ϕ_0 from Eq. (B15), Eq. (B16), and Eq. (B18), respectively. In the main text, this form is compared favorably with the exact current evaluated by solving the equations numerically.

APPENDIX C: EXTRACTING THE FREQUENCIES OF THE AC JOSEPHSON CURRENT

The Josephson current for a fractionalized PDW state shows a beatlike structure. This suggests multiple frequencies are contributing to the AC Josephson current. This section provides the details to obtain the Josephson current frequencies. To do so, we need to perform a Fourier transform of the AC Josephson current to the frequency domain.

We simplify Eq. (B21) by assuming that the interjunction PP to PH hopping amplitude is small compared to the intrajunction hoppings, i.e., $t_1 \ll t_0$. In an experimental scenario, this requires using a barrier to decay the PH hoppings across the junction. However, for a finite but small t_1, this will not create any qualitative difference to the discussion below. Also, in a long-time limit, the transient current regime from the CDW vanishes, i.e., $\theta_0' \to 0$. Hence the current reduces to

$$I_J \approx \frac{2\kappa n}{\hbar} \sin \theta_0 + \frac{2t_0 \sqrt{nn'}}{\hbar} \cos \frac{\phi_0}{2} \sin \frac{\theta_0}{2}$$
$$- \frac{2t_0}{\pi \hbar} \sqrt{\frac{n'}{n}} \sin \frac{\phi_0}{2} \sin \frac{\theta_0}{2}. \tag{C1}$$

Furthermore, since $n \approx n'$, the second term dominates over the third. The expression for the current further simplifies to

$$I_J \approx \frac{2\kappa n}{\hbar} \sin \theta_0 + \frac{2t_0 \sqrt{nn'}}{\hbar} \cos \frac{\phi_0}{2} \sin \frac{\theta_0}{2}. \tag{C2}$$

Using trigonometric identities, the second term becomes

$$I_2 \approx \frac{t_0 \sqrt{nn'}}{\hbar} \left[\sin \left(\frac{\theta_0 + \phi_0}{2} \right) + \sin \left(\frac{\theta_0 - \phi_0}{2} \right) \right]. \tag{C3}$$

Here θ_0 and ϕ_0 are given by Eq. (B15) and Eq. (B18), respectively. The constant terms do not contribute to the frequency of the AC Josephson frequency, and hence we can ignore them for the following analysis. Next we make a series expansion for the Ci[...] function and neglecting the constant and higher-order terms, we obtain

$$I_2 \approx \frac{t_0 \sqrt{nn'}}{\hbar} [\sin (a_+ + b \sin \xi t) + \sin (a_- - b \sin \xi t)], \tag{C4}$$

where we have defined

$$a_{\pm} = \frac{1}{2}\left(\frac{2\mu_{\Delta}}{\hbar} \pm \frac{\eta}{\hbar} \pm \frac{2\kappa'}{\hbar}\right), \quad \text{(C5)}$$

$$b = \frac{\kappa}{2\mu_{\Delta}}, \quad \text{(C6)}$$

$$\xi = \frac{2\mu_{\Delta}}{\hbar}. \quad \text{(C7)}$$

Next, we expand

$$\cos(x\sin\theta) = \mathcal{J}_0(x) + 2\sum_{p=1}^{\infty}\mathcal{J}_{2p}(x)\cos(2p\theta), \quad \text{(C8)}$$

$$\sin(x\sin\theta) = 2\sum_{p=1}^{\infty}\mathcal{J}_{2p+1}(x)\sin[(2p+1)\theta], \quad \text{(C9)}$$

where $\mathcal{J}_\nu(x)$ is the Bessel function of the first kind of the νth order. Neglecting the higher-order terms the current in Eq. (C1) becomes

$$\begin{aligned} I_J &\approx \frac{t_0\sqrt{nn'}}{\hbar}(\mathcal{J}_0(b)(\sin a_+ t + \sin a_- t) \\ &+ \mathcal{J}_1(b)\{\sin[(a_+ + \xi)t] - \sin[(a_- + \xi)t] \\ &+ \sin a_- t - \sin a_+ t\}) + \frac{2\kappa n}{\hbar}\sin \xi t. \end{aligned} \quad \text{(C10)}$$

Since all the terms are directly proportional to t, one can easily read off the frequencies for the AC current, by performing a Fourier transform. This is given by

$$\begin{aligned} \tilde{I}_J(\omega) &= \frac{\kappa n}{\hbar}\delta(\omega - \xi) + \frac{t_0\sqrt{nn'}}{2\hbar}\{[\mathcal{J}_0(b) + \mathcal{J}_1(b)]\delta(\omega - a_-) \\ &+ \mathcal{J}_1(b)\delta(\omega - a_+ - \xi) - \mathcal{J}_1(b)\delta(\omega - a_- - \xi) \\ &+ [\mathcal{J}_0(b) - \mathcal{J}_1(b)]\delta(\omega - a_-)\}. \end{aligned} \quad \text{(C11)}$$

The primary frequency ξ is the usual AC Josephson frequency. The other frequencies are the additional ones originating due to the entanglement of the two orders. The ratio of the primary to the few additional frequencies is given by

$$\frac{\omega_1}{\omega_0} = \frac{1}{2} - \left(\frac{\eta + 2\kappa'}{4eU}\right), \quad \text{(C12)}$$

$$\frac{\omega_4}{\omega_0} = \frac{1}{2} + \left(\frac{\eta + 2\kappa'}{4eU}\right), \quad \text{(C13)}$$

$$\frac{\omega_2}{\omega_0} = \frac{3}{2} + \left(\frac{\eta + 2\kappa'}{4eU}\right), \quad \text{(C14)}$$

$$\frac{\omega_3}{\omega_0} = \frac{3}{2} - \left(\frac{\eta + 2\kappa'}{4eU}\right), \quad \text{(C15)}$$

where ω_{i-1} are the ith delta function peak of Eq. (C11). For large potential difference between the two junctions, i.e., $U \gg \eta + 2\kappa'$, the second term of all the ratios vanishes. Moreover, the ratio between the primary and additional frequencies will occur at half-odd integers, i.e., $1/2, 3/2, 5/2, \ldots$. However, the peak strength will diminish for the higher-order term as it is determined by the higher-order Bessel function. Studying such frequency dependence of the AC Josephson current will give an indication of the fractionalized PDW order.

APPENDIX D: EXTRACTING THE ENVELOPE

The Josephson current for a PDW state or fractionalized PDW state shows a beatlike structure. Such a beatlike form can be distinguished in experiments establishing an entanglement between the superconducting and the charge orders. To provide a detailed description, it becomes necessary to determine the parameters that control such a current envelope. In this section, we provide the details of the envelope of the Josephson current. We start with Eq. (C2). Using trigonometric identities, we obtain

$$\begin{aligned} I_J &= \frac{\kappa n}{\hbar}\sin\theta_0 + \frac{t_0\sqrt{nn'}}{\hbar}\sin\left(\theta_0 + \frac{\phi_0 - \theta_0}{2}\right) \\ &+ \frac{\kappa n}{\hbar}\sin\theta_0 + \frac{t_0\sqrt{nn'}}{\hbar}\sin\left(\theta_0 - \frac{\phi_0 + \theta_0}{2}\right). \end{aligned} \quad \text{(D1)}$$

Before adding the sine waves we define $(\phi_0 - \theta_0)/2 = \chi_1$ and $(\phi_0 + \theta_0)/2 = \chi_2$. Therefore, using $n \approx n'$, the expression current becomes

$$\begin{aligned} I_J &= \frac{n}{\hbar}\Big[\sqrt{\kappa^2 + t_0^2 + 2\kappa t_0\cos\chi_1}\sin(\theta_0 + \xi_1) \\ &+ \sqrt{\kappa^2 + t_0^2 + 2\kappa t_0\cos\chi_2}\sin(\theta_0 - \xi_2)\Big]. \end{aligned} \quad \text{(D2)}$$

Here the phase angles ξ_i are given by

$$\xi_i = \sin^{-1}\left(\frac{t_0\sin\chi_i}{\sqrt{\kappa^2 + t_0^2 + 2\kappa t_0\cos\chi_i}}\right), \quad \text{(D3)}$$

where $i = 1, 2$. In the perturbative limit, t_0 is the small parameter in our calculations; the phase shifts can be assumed to be small, such that $\xi_i = 0$. Therefore the current becomes

$$I_J = \frac{n}{\hbar}\sum_{i=1}^{2}\Big[\sqrt{\kappa^2 + t_0^2 + 2\kappa t_0\cos\chi_i}\Big]\sin(\theta_0). \quad \text{(D4)}$$

Here the amplitude of the envelope is controlled by two phases. The faster oscillation is governed by $\chi_2 = (\phi_0 + \theta_0)/2$ and the slower one by $\chi_1 = (\phi_0 - \theta_0)/2$. The total envelope is the sum of the square root term in Eq. (D4), and therefore contains further oscillations given by χ_1 and χ_2.

APPENDIX E: JOSEPHSON CURRENT WITH DEPHASING PARAMETER

1. Electric field parallel to Q_0

This Appendix discusses the procedure to obtain the average Josephson current with the dephasing parameter. Initially at $t = 0$, the phase of the CDW order is given by $\theta'(0) = Q_0\delta = C_2$. Similarly, one can set $\phi(0) = Q_0\delta + \gamma$, where γ is a constant. The zeroth-order solution for ϕ thus becomes

$$\begin{aligned} \phi_0 &= -\frac{\eta}{\hbar}t + (Q_0\delta + \gamma) + \frac{2\kappa'}{r_0\hbar}\text{Ci}[Q_0\delta e^{-r_0 t}] \\ &- \frac{\kappa}{\mu_{\Delta}}\sin\left(\frac{2\mu_{\Delta}}{\hbar}t + C_1\right). \end{aligned} \quad \text{(E1)}$$

Putting this in Eq. (18), we obtain the $I_J(t)$, which we integrate numerically over a fixed time to get the average $\langle I_J \rangle$. Notice that the cosine-integral dependence of δ in ϕ_0 generates a
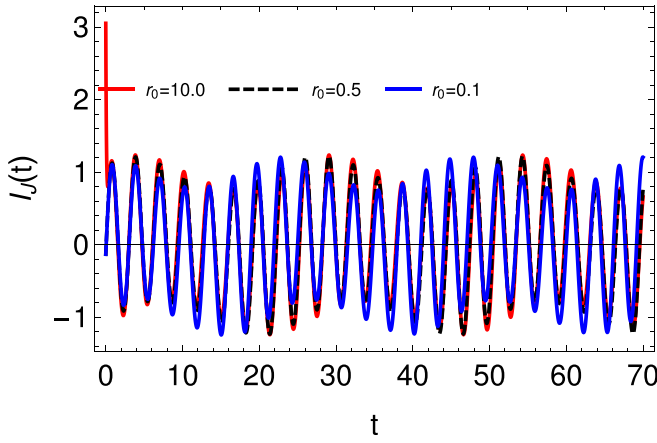
FIG. 8. The AC Josephson current for different values of r_0. The beatlike structure for the AC current remains robust for all the values of r_0. Only the initial transient nature of the current vanishes for smaller r_0.

higher harmonics of oscillation of $\langle I_J \rangle$ with δ. Thus, it becomes difficult to extract the PDW modulation wave vector in this setup.

2. Electric field perpendicular to Q_0

No such complications arise when the JJ is set up such that the wave vector is perpendicular to the electric field. In this case, although $r_0 = \eta = 0$ and the transient current cannot survive, the initial $\theta_0'(0) = Q_0\delta$. Similarly, one can set $\phi(0) = Q_0\delta + \gamma$, where γ is a constant. Here δ denotes the phase difference between the CDW wave vector in the two terminals. Consequently, the zeroth-order solutions become

$$\theta_0 = \frac{2\mu_\Delta}{\hbar} t + C_1, \tag{E2}$$

$$\theta_0' = Q_0\delta, \tag{E3}$$

$$\phi_0 = (Q_0\delta + \gamma) - \frac{2\kappa'}{\hbar}\cos(Q_0\delta)t - \frac{\kappa}{\mu_\Delta}\sin\left(\frac{2\mu_\Delta}{\hbar}t + C_1\right). \tag{E4}$$

Putting these expressions in Eq. (18), we can evaluate average current, which shows clear modulations with δ.

APPENDIX F: CURRENT DUE TO CDW PHASE

The CDW phase can be strongly pinned by the boundary of the junctions and the disorder of the samples. However, here we consider the general possibility for the current arising due to the phase of the CDW order. We note that the term $V_A - V_B = -(eEn'/Q_0)\theta' \equiv -r_0\theta'$ generates only a transient current response at short times. The parameter r_0 characterizes the strength of the phase current from the CDW. The long-time behavior of the AC Josephson current remains invariant when we vary this term. In Fig. 8, we have shown the evolution of the AC Josephson current for the PDW scenario. The parameters used here are the same as those presented in Fig. 2(b) of the main text. As we increase r_0, the AC response changes for $t \to 0$, whereas it remains invariant at long times. The frequency of the oscillation is independent of r_0 and thus remains the same. The amplitude of the oscillation changes weakly when $r_0 < 1$. Therefore, the results presented in the paper remain robust while we change this parameter.

APPENDIX G: JOSEPHSON CURRENT WITH COMPLEX HOPPINGS

Here we consider the complex hoppings between the particle-particle and particle-hole hoppings. Since this term is connected by the PDW order, it can be complex in general. We confirm here whether the imaginary part of these hoppings considerably modifies our results.

The set of Schrödinger's equations is written, with $\overline{\psi} = (\sqrt{n_A}e^{i\theta_A}, \sqrt{n_B}e^{i\theta_B}, \sqrt{n_A'}e^{i\theta_A'}, \sqrt{n_B'}e^{i\theta_B'})$,

$$i\hbar \frac{\partial}{\partial t}\psi = \begin{pmatrix} \mu_\Delta & \kappa & t_0 & t_1 \\ \kappa & -\mu_\Delta & t_1 & t_0 \\ t_0^* & t_1^* & V_A & \kappa' \\ t_1^* & t_0^* & \kappa' & V_B \end{pmatrix}\psi. \tag{G1}$$

By following the procedure similar to Appendix A, we arrive at the set of Schrödinger equations

$$\frac{\partial \bar{n}}{\partial t} = \frac{4}{\hbar}\left\{-\kappa n\sin\theta + \sqrt{nn'}\left[\cos\frac{\phi}{2}\left(\text{Re}\,t_0\sin\frac{\theta'-\theta}{2} - \text{Re}\,t_1\sin\frac{\theta'+\theta}{2}\right) - \sin\frac{\phi}{2}\left(\text{Im}\,t_0\sin\frac{\theta'-\theta}{2} - \text{Im}\,t_1\sin\frac{\theta'+\theta}{2}\right)\right]\right\}, \tag{G2}$$

$$\frac{\partial \theta}{\partial t} = \frac{2}{\hbar}\left\{\mu_\Delta + \sqrt{\frac{n'}{n}}\left[\sin\frac{\phi}{2}\left(\text{Re}\,t_0\sin\frac{\theta'-\theta}{2} - \text{Re}\,t_1\sin\frac{\theta'+\theta}{2}\right) - \cos\frac{\phi}{2}\left(\text{Im}\,t_0\sin\frac{\theta'-\theta}{2} - \text{Im}\,t_1\sin\frac{\theta'+\theta}{2}\right)\right]\right\}, \tag{G3}$$

$$\frac{\partial \bar{n}'}{\partial t} = \frac{4}{\hbar}\left\{-\kappa'n'\sin\theta' + \sqrt{nn'}\left[\cos\frac{\phi}{2}\left(\text{Re}\,t_0\sin\frac{\theta-\theta'}{2} - \text{Re}\,t_1\sin\frac{\theta'+\theta}{2}\right) - \sin\frac{\phi}{2}\left(\text{Im}\,t_0\sin\frac{\theta-\theta'}{2} - \text{Im}\,t_1\sin\frac{\theta'+\theta}{2}\right)\right]\right\}, \tag{G4}$$

$$\frac{\partial \theta'}{\partial t} = \frac{1}{\hbar}\left\{V_A - V_B - 2\sqrt{\frac{n}{n'}}\left[\sin\frac{\phi}{2}\left(\text{Re}\,t_0\sin\frac{\theta-\theta'}{2} - \text{Re}\,t_1\sin\frac{\theta'+\theta}{2}\right) - \cos\frac{\phi}{2}\left(\text{Im}\,t_0\sin\frac{\theta-\theta'}{2} - \text{Im}\,t_1\sin\frac{\theta'+\theta}{2}\right)\right]\right\}, \tag{G5}$$

$$\frac{\partial \phi}{\partial t} = -\frac{1}{\hbar}[\eta + 2\kappa\cos\theta + 2\kappa'\cos\theta']. \tag{G6}$$
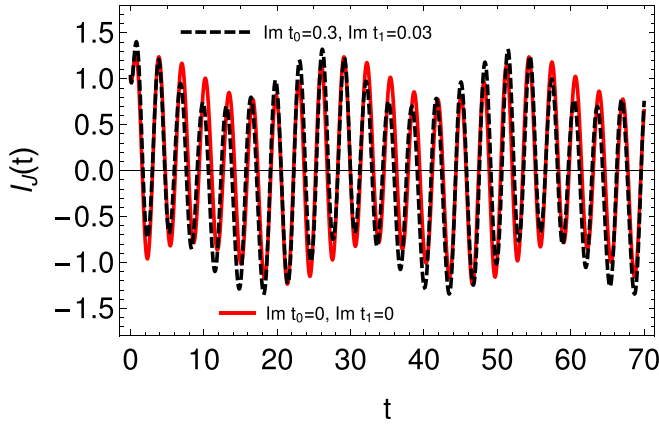
FIG. 9. AC Josephson current for two scenarios. In both, $\text{Re}\, t_0 = 0.3$ and $\text{Re}\, t_1 = 0.03$. Moreover, all other parameters are the same as those used in Fig. 2(b). The dashed lines manifest the effects of the imaginary part of t_0, and t_1 is finite. Although the amplitude of the current changes slightly as we increase the imaginary part of the hoppings, the oscillation frequencies remain the same.

We solve the equations numerically and derive the Josephson current using Eq. (16). The results are presented in Fig. 9.

This shows that the Josephson current as the imaginary part of the hoppings is increased. Although the amplitude of the current changes with the increasing imaginary part of the hoppings, the frequency remains the same. The oscillation frequencies in Eqs. (27)–(30) are independent of the t_0 and t_1. Consequently, our other results presented in the main paper remain robust if we consider these hoppings to be complex. The results are also expected to hold even if we consider different values for t_0 in two terminals.

APPENDIX H: SHAPIRO SPIKES

The main paper shows the qualitative voltage-current characteristics in a current-driven Josephson circuit, similar to the experimental situation. Here we present the Shapiro spikes for the voltage-driven Josephson systems for completeness. In this setup, the current shows sharp δ peaks at the integer
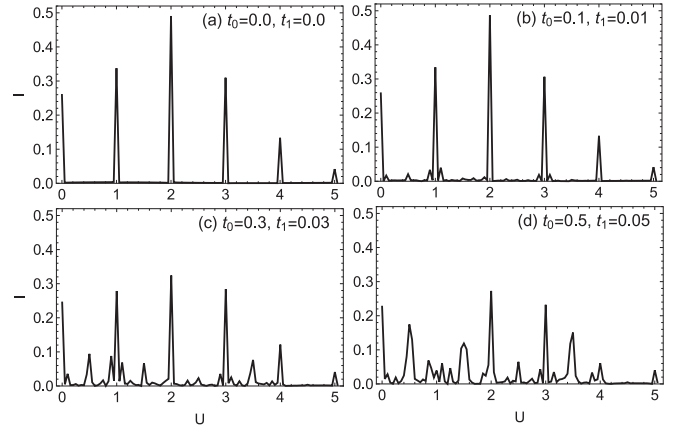

FIG. 10. Demonstration of the total DC current with the applied DC voltage U across the junctions in the inverse Josephson setup. In (a) we set $t_0 = 0$, $t_1 = 0$ the parameter corresponding to the simple coexistence of CDW and SC orders. The sharp Shapiro spikes can be observed when the applied DC voltage U is equal to the integer multiple of the applied frequency ω. In (b)–(d) we plot the same for finite t_0, t_1 which corresponds to the fractionalized PDW scenario. In (b) t_0, t_1 is small, and other peaks start developing in between the two Shapiro spikes. In (c) and (d) these additional peaks become stronger as the entanglement between the two orders is increased.

multiples of the AC frequency ω which is set to unity. These peaks are known as Shapiro spikes.

For the coexistence of orders t_0, $t_1 = 0$ and we find in Fig. 10(a) the expected sharp Shapiro spikes at the integer multiple of ω. We also solve Eqs. (8)–(13) numerically for an AC voltage of the same form but a finite t_0, t_1 and track the evolution of the Shapiro spikes. In Fig. 10(b) we present the results for a weak entanglement between the two orders. We see that multiple weak peaks emerge as soon as the entanglement between the two orders increases. Such extra peaks get stronger as the overlap between the charge and SC order becomes large in Fig. 10(c). Finally, for a strong fractionalized PDW state, the Shapiro spikes appear at different DC voltage than the integer multiple of ω. For instance, a spike appears at $U = 1/2$ in Fig. 10(d) whereas the expected integer spike at $U = 1$ completely vanishes.

[1] H. Alloul, T. Ohno, and P. Mendels, Phys. Rev. Lett. **63**, 1700 (1989).

[2] H. Alloul, P. Mendels, H. Casalta, J. F. Marucco, and J. Arabski, Phys. Rev. Lett. **67**, 3140 (1991).

[3] W. W. Warren, Jr., R. E. Walstedt, G. F. Brennert, R. J. Cava, R. Tycko, R. F. Bell, and G. Dabbagh, Phys. Rev. Lett. **62**, 1193 (1989).

[4] B. Loret, N. Auvray, Y. Gallais, M. Cazayous, A. Forget, D. Colson, M.-H. Julien, I. Paul, M. Civelli, and A. Sacuto, Nat. Phys. **15**, 771 (2019).

[5] R. M. Fernandes, P. P. Orth, and J. Schmalian, Annu. Rev. Condens. Matter Phys. **10**, 133 (2019).

[6] E. Fradkin, S. A. Kivelson, and J. M. Tranquada, Rev. Mod. Phys. **87**, 457 (2015).

[7] S. Sachdev and R. La Placa, Phys. Rev. Lett. **111**, 027202 (2013).

[8] A. Allais, D. Chowdhury, and S. Sachdev, Nat. Commun. **5**, 5771 (2014).

[9] A. Allais, J. Bauer, and S. Sachdev, Phys. Rev. B **90**, 155114 (2014).

[10] C.-C. Chien, Y. He, Q. Chen, and K. Levin, Phys. Rev. B **79**, 214527 (2009).

[11] Z. Du, H. Li, S. H. Joo, E. P. Donoway, J. Lee, J. C. S. Davis, G. Gu, P. D. Johnson, and K. Fujita, Nature (London) **580**, 65 (2020).

[12] Z. Shi, P. G. Baity, J. Terzic, T. Sasagawa, and D. Popović, Nat. Commun. **11**, 3323 (2020).

[13] P. M. Lozano, G. D. Gu, J. M. Tranquada, and Q. Li, Phys. Rev. B **103**, L020502 (2021).

[14] M. S. Scheurer, S. Chatterjee, W. Wu, M. Ferrero, A. Georges, and S. Sachdev, Proc. Natl. Acad. Sci. USA **115**, E3665 (2018).

[15] S. Sachdev, H. D. Scammell, M. S. Scheurer, and G. Tarnopolsky, Phys. Rev. B **99**, 054516 (2019).

[16] Z. Nussinov and J. Zaanen, J. Phys. IV **12**, 245 (2002).

[17] J. Zaanen and Z. Nussinov, Phys. Status Solidi B **236**, 332 (2003).

[18] P. A. Lee, N. Nagaosa, T.-K. Ng, and X.-G. Wen, Phys. Rev. B **57**, 6003 (1998).

[19] Z. Dai, Y.-H. Zhang, T. Senthil, and P. A. Lee, Phys. Rev. B **97**, 174511 (2018).

[20] Y. Wang, D. F. Agterberg, and A. Chubukov, Phys. Rev. B **91**, 115103 (2015).

[21] S. A. Hartnoll, A. Lucas, and S. Sachdev, *Holographic Quantum Matter* (MIT Press, Cambridge, Massachusetts, 2018).

[22] D. Chakraborty, M. Grandadam, M. H. Hamidian, J. C. S. Davis, Y. Sidis, and C. Pépin, Phys. Rev. B **100**, 224511 (2019).

[23] M. Grandadam, D. Chakraborty, and C. Pépin, J. Supercond. Novel Magn. **33**, 2361 (2020).

[24] C. Pépin, D. Chakraborty, M. Grandadam, and S. Sarkar, Annu. Rev. Condens. Matter Phys. **11**, 301 (2020).

[25] M. Grandadam, D. Chakraborty, X. Montiel, and C. Pépin, Phys. Rev. B **102**, 121104(R) (2020).

[26] M. H. Hamidian, S. D. Edkins, S. H. Joo, A. Kostin, H. Eisaki, S. Uchida, M. J. Lawler, E.-A. Kim, A. P. Mackenzie, K. Fujita, J. Lee, and J. C. S. Davis, Nature (London) **532**, 343 (2016).

[27] J. E. Hoffman, E. W. Hudson, K. M. Lang, V. Madhavan, H. Eisaki, S. Uchida, and J. C. Davis, Science **295**, 466 (2002).

[28] W. D. Wise, M. C. Boyer, K. Chatterjee, T. Kondo, T. Takeuchi, H. Ikuta, Y. Wang, and E. W. Hudson, Nat. Phys. **4**, 696 (2008).

[29] J.-J. Wen, H. Huang, S.-J. Lee, H. Jang, J. Knight, Y. S. Lee, M. Fujita, K. M. Suzuki, S. Asano, S. A. Kivelson, C.-C. Kao, and J.-S. Lee, Nat. Commun. **10**, 3269 (2019).

[30] T. Wu, H. Mayaffre, S. Krämer, M. Horvatić, C. Berthier, W. N. Hardy, R. Liang, D. A. Bonn, and M.-H. Julien, Nat. Commun. **6**, 6438 (2015).

[31] J. Q. Lin, H. Miao, D. G. Mazzone, G. D. Gu, A. Nag, A. C. Walters, M. García-Fernández, A. Barbour, J. Pelliciari, I. Jarrige, M. Oda, K. Kurosawa, N. Momono, K.-J. Zhou, V. Bisogni, X. Liu, and M. P. M. Dean, Phys. Rev. Lett. **124**, 207005 (2020).

[32] G. Baskaran and P. W. Anderson, Phys. Rev. B **37**, 580 (1988).

[33] P. A. Lee and N. Nagaosa, Phys. Rev. B **46**, 5621 (1992).

[34] K.-Y. Yang, W. Q. Chen, T. M. Rice, M. Sigrist, and F.-C. Zhang, New J. Phys. **11**, 055053 (2009).

[35] A. Perelomov, Physica D **4**, 1 (1981).

[36] D. F. Agterberg, J. S. Davis, S. D. Edkins, E. Fradkin, D. J. Van Harlingen, S. A. Kivelson, P. A. Lee, L. Radzihovsky, J. M. Tranquada, and Y. Wang, Annu. Rev. Condens. Matter Phys. **11**, 231 (2020).

[37] P. Corboz, T. M. Rice, and M. Troyer, Phys. Rev. Lett. **113**, 046402 (2014).

[38] P. Choubey, W.-L. Tu, T.-K. Lee, and P. J. Hirschfeld, New J. Phys. **19**, 013028 (2017).

[39] N. Doiron-Leyraud, C. Proust, D. LeBoeuf, J. Levallois, J.-B. Bonnemaison, R. Liang, D. A. Bonn, W. N. Hardy, and L. Taillefer, Nature (London) **447**, 565 (2007).

[40] S. Blanco-Canosa, A. Frano, T. Loew, Y. Lu, J. Porras, G. Ghiringhelli, M. Minola, C. Mazzoli, L. Braicovich, E. Schierle, E. Weschke, M. Le Tacon, and B. Keimer, Phys. Rev. Lett. **110**, 187001 (2013).

[41] S. E. Sebastian, N. Harrison, R. Liang, D. A. Bonn, W. N. Hardy, C. H. Mielke, and G. G. Lonzarich, Phys. Rev. Lett. **108**, 196403 (2012).

[42] J. Chang, E. Blackburn, O. Ivashko, A. T. Holmes, N. B. Christensen, M. Hucker, R. Liang, D. A. Bonn, W. N. Hardy, U. Rutt, M. v. Zimmermann, E. M. Forgan, and H. S. M., Nat. Commun. **7**, 11494 (2016).

[43] T. Wu, H. Mayaffre, S. Krämer, M. Horvatic, C. Berthier, W. N. Hardy, R. Liang, D. A. Bonn, and M.-H. Julien, Nature (London) **477**, 191 (2011).

[44] S. Gerber, H. Jang, H. Nojiri, S. Matsuzawa, H. Yasumura, D. A. Bonn, R. Liang, W. N. Hardy, Z. Islam, A. Mehta, S. Song, M. Sikorski, D. Stefanescu, Y. Feng, S. A. Kivelson, T. P. Devereaux, Z.-X. Shen, C. C. Kao, W. S. Lee, D. Zhu *et al.*, Science **350**, 949 (2015).

[45] T. Machida, Y. Kohsaka, K. Matsuoka, K. Iwaya, T. Hanaguri, and T. Tamegai, Nat. Commun. **7**, 11747 (2016).

[46] D. H. Torchinsky, F. Mahmood, A. T. Bollinger, I. Božović, and N. Gedik, Nat. Mater. **12**, 387 (2013).

[47] L. Nie, G. Tarjus, and S. A. Kivelson, Proc. Natl. Acad. Sci. USA **111**, 7980 (2014).

[48] L. Nie, Lauren E. Hayward Sierens, R. G. Melko, S. Sachdev, and S. A. Kivelson, Phys. Rev. B **92**, 174505 (2015).

[49] A. Banerjee, A. Garg, and A. Ghosal, Phys. Rev. B **98**, 104206 (2018).

[50] G. Campi, A. Bianconi, N. Poccia, G. Bianconi, L. Barba, G. Arrighetti, D. Innocenti, J. Karpinski, N. D. Zhigadlo, S. M. Kazakov, M. Burghammer, M. V. Zimmermann, M. Sprung, and A. Ricci, Nature (London) **525**, 359 (2015).

[51] S. D. Edkins, A. Kostin, K. Fujita, A. P. Mackenzie, H. Eisaki, S. Uchida, S. Sachdev, M. J. Lawler, E.-A. Kim, J. C. S. Davis, and M. H. Hamidian, Science **364**, 976 (2019).

[52] A. Barone and G. Paterno, *Physics and Applications of the Josephson Effect* (Wiley, New York, 1982).

[53] G. Grüner, Rev. Mod. Phys. **60**, 1129 (1988).

[54] P. A. Lee and T. M. Rice, Phys. Rev. B **19**, 3970 (1979).

[55] R. Comin, R. Sutarto, E. H. da Silva Neto, L. Chauviere, R. Liang, W. N. Hardy, D. A. Bonn, F. He, G. A. Sawatzky, and A. Damascelli, Science **347**, 1335 (2015).